FIFI LS: a Far-Infrared 3D Spectral Imager for SOFIA

L. W. Looney[a], W. Raab[a], A. Poglitsch[a], N. Geis[a], D. Rosenthal[a],
R. Hönle[a], R. Klein[b], F. Fumi[a], R. Genzel[a], T. Henning[b]

[a]Max-Planck-Institut für Extraterrestrische Physik (MPE), Postfach 1603,
D-85740 Garching, Germany
[b]Friedrich-Schiller Astronomisches Institut Universität, Jena, Schillergäßchen 3,
D-07745 Jena, Germany

ABSTRACT

FIFI LS is a far-infrared integral field spectrometer for SOFIA that maximizes observing efficiency by spectrally imaging fields in two medium velocity resolution bands simultaneously and nearly independently. Although the two observing bands, Red (110-210 microns) and Blue (42-110 microns), share some common fore-optics, the Field-Imaging Far-Infrared Line Spectrometer (FIFI LS) can observe diffraction-limited spectra at R = 1400 to 6500, depending on wavelength, with two separate Littrow mounted spectrometers. To further increase the observing efficiency, we employ an integral field technique that allows multiplexing spatially. This is achieved by utilizing slicer mirrors to optically re-arrange the 2D field into a single slit for a standard long slit spectrometer. Effectively, a 5 × 5 pixel spatial field of view is imaged to a 25 × 1 pixel slit and dispersed to a 25 × 16 pixel, 2D detector array. The detectors are two large format Ge:Ga arrays, axially stressed in the Red channel to achieve a longer wavelength response and slightly stressed in the Blue channel. Overall, for each of the 25 spatial pixels in each band, the instrument can cover a velocity range of approximately 1500 km/s with an estimated sensitivity of 2×10^{-15} W $Hz^{1/2}$ per pixel. This arrangement provides good spectral coverage with high responsivity. With this scheme FIFI LS will have advantages over single-slit spectrometers in detailed morphological studies of the heating and cooling of galaxies, star formation, the ISM under low-metalicity conditions as found in dwarf galaxies, active galactic nuclei and their environment, starbursts, and merging/interacting galaxies.

Keywords: Integral Field Imaging, Spectrometer, Far-Infrared, grating, optical slicer, FIR, FIFI LS, FIFI, SOFIA

1. INTRODUCTION

Far-infrared astronomy will take a major step forward with the unprecedented spatial resolution and sensitivity that the Stratospheric Observatory For Infrared Astronomy (SOFIA) can offer. Far-infrared astronomical observations are impossible from the ground due to water absorption, requiring stratospheric or space observatories. However, they provide an essential probe of astrophysical conditions in areas of interest that are mostly inaccessible at other wavelengths due to severe extinction from interstellar dust or when the intrinsic physics of the source is manifest at far-infrared wavelengths. In particular far-infrared spectroscopy on SOFIA, which was pioneered and developed on SOFIA's predecessor the Kuiper Airborne Observatory (KAO) and greatly extended with the Infrared Space Observatory (ISO), will inject crucial data into many astrophysical fields.

We have built upon the success of our KAO far-infrared Fabry-Perot spectrometer (FIFI[1,2]) to develop an advanced far-infrared spectrometer that can take advantage of the major improvements with SOFIA. The Field-Imaging Far-Infrared Line Spectrometer (FIFI LS[3–5]) performs integral field spectral imaging in two nearly independent wavelength bands: 42 to 110 μm and 110 to 210 μm. This will allow the instrument to simultaneously obtain dual wavelength band, spectral imaging of a 5 × 5 pixel field, without scanning a Fabry-Perot or multiple pointings of a long-slit spectrometer.

With FIFI LS our main scientific goals will include detailed morphological studies of: (1) the heating and cooling of galaxies, (2) star formation and the interstellar medium under low-metalicity conditions, as found in dwarf galaxies, (3) active galactic nuclei and their environment, (4) merging and interacting galaxies, (5) large surveys of nearby galaxies, and (6) ultra-luminous infrared galaxies. Overall, FIFI LS on SOFIA will be more sensitive than the ISO Long-Wavelength Spectrometer and have much higher spatial resolution and mapping capabilities. As a future option, an extension of the instrument to the 25-42 μm and >300 μm ranges is planned based upon availability of Si:Sb arrays developed for SIRTF and GaAs blocked impurity band arrays, respectively.

email: lwl@mpe.mpg.de; http://fifi-ls.mpe-garching.mpg.de

Airborne Telescope Systems II, Ramsey K. Melugin, Hans-Peter Röser, Editors,
Proceedings of SPIE Vol. 4857 (2003) © 2003 SPIE · 0277-786X/03/$15.00

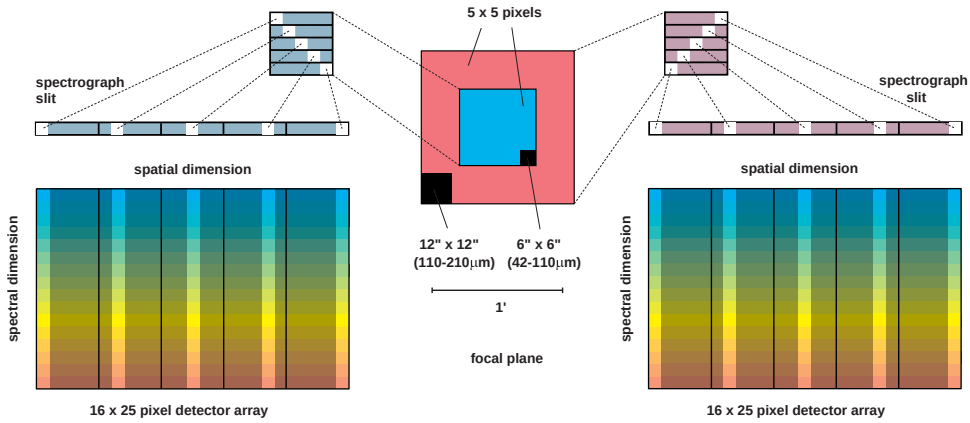

Figure 1. Focal plane projections of the long and short wavelength channels of FIFI LS, showing the instantaneous field of view for both channels, the re-arrangement of the 5 × 5 field of view onto a 25 × 1 slit, and the spectral projection of the integral field onto the 16 × 25 detector arrays.

2. SPECTROMETER CONCEPT

To achieve the astrophysical objectives of FIFI LS, very high observing sensitivities and efficiencies are essential. One of the ways we accomplish this is to chose a comparably medium spectral resolution (R ∼2000) such that FIFI LS does not require more than 1 grating and no predisperser; yet it is still sufficient for the velocity dispersion of our preferred sources. In addition, FIFI LS utilizes two nearly independent waveband channels: Blue (42 to 110 μm) and Red (110 to 210 μm). The main reason for this is to allow for simultaneous observation of two far infrared lines that are necessary to infer physical conditions in the astronomical source, such as temperature or density. The most novel technique of FIFI LS to increase its efficiency is by utilizing integral field spectroscopy in each wavelength band. This allows 2-dimensional spatial mapping and simultaneous spectral multiplexing by optically slicing, or re-arranging, the 2D 5 × 5 pixel field of view of FIFI LS into a single 1D 25 × 1 pixel slit. From that point onward, the spectrometer uses a traditional long-slit reflective grating spectrometer technique that disperses the slit onto a 2D 16 × 25 pixel detector array.[6–8] Fig. 2 shows graphically the integral field concept for concurrent observations in the Blue and Red channels. Although "optical slicers" have been used for solar spectroscopy[9] and more recently successfully implemented for near-infrared astronomy,[10] this is the first time that this technique has been applied in the far-infrared. For further discussion of the FIFI LS optics and the effects of diffraction caused by the slicer mirrors, see this volume.[11]

3. INSTRUMENT DESIGN

3.1. Cryostat

The FIFI LS instrument is directly attached to the science instrument mounting flange of the SOFIA telescope. In Fig. 2, a 3D colorized model of a cut through the FIFI LS instrument is shown. The instrument is comprised of a vacuum vessel and attachment cradle that assists in supporting FIFI LS on the telescope flange. The vacuum vessel is roughly a 1 m × 1 m × 1 m shell that contains three cryogen vessels, all of the optics, and the two detectors. Mounted to the bottom of the vacuum vessel are the dichroic beam splitter and the field optics for the focal plane guiding camera. The dichroic filter separates the telescope's light into the two beams: the optical, directed downward into the telescope guiding camera, and the infrared, directed upward into the cryostat. The infrared beam from the telescope enters the vacuum vessel through a polyethylene window, which also serves as a pressure barrier between stratospheric pressure and the vacuum inside the instrument.

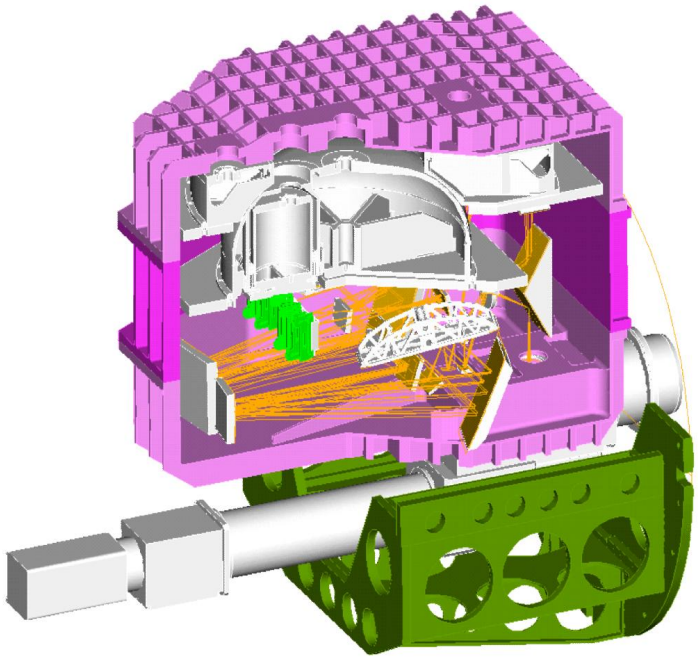

Figure 2. Solid model of the FIFI LS system, with a cutout to illustrate the inner components. FIFI LS is mounted to the SOFIA instrument flange on the right side. This image shows the three cryogenic containers (top-most), the optical worksurfaces (hanging from the cryogenic containers via G-10 tabs), the optics, and the guiding camera (bottom-most).

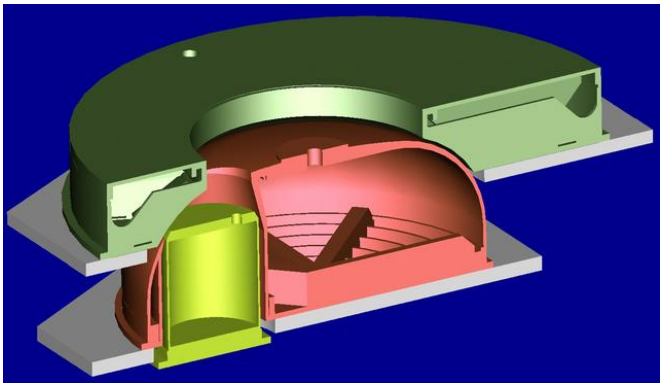

Figure 3. Solid model of the three cryogenic containers, from top to bottom: liquid nitrogen, liquid helium, and the smaller superfluid helium.

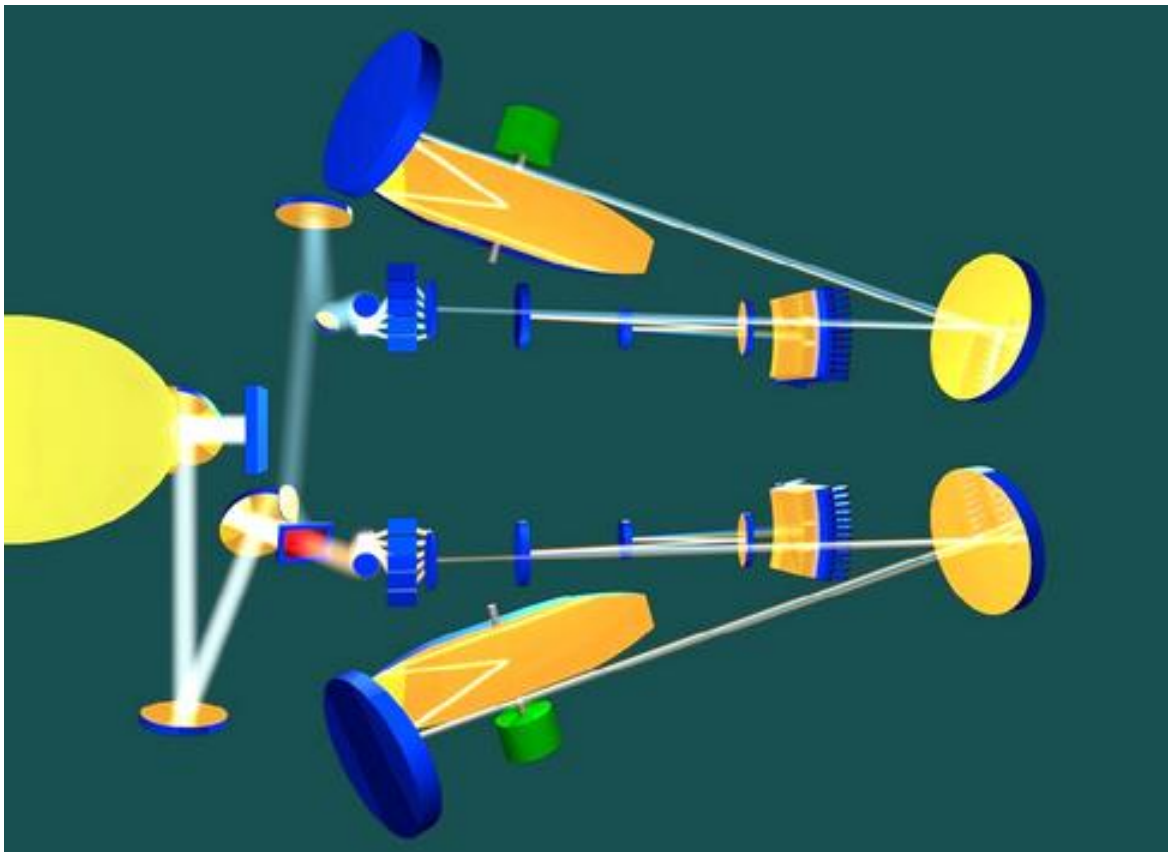

Figure 4. Solid model of the FIFI LS optical system, viewed from the bottom. The IR beam enters from the left and is split by a dichroic into the long and short spectrometers— the upper is for the Blue band (short λ) and the lower is for the Red band (long λ). The 16 $\times$ 25 detector arrays are the biconic surfaces, second from the right.

There are three cryogenic containers in FIFI LS for liquid nitrogen, liquid helium, and superfluid helium (a small pumped reservoir of liquid helium). The manner in which the three vessels are mounted together is shown in Fig. 3, a center cut through the cryogenic vessels. The liquid nitrogen container has a capacity of 25 liters, which provides cooling for the outer radiation shields, the liquid nitrogen worksurface, and the entrance optics (i.e. a K-mirror assembly for field rotation correction and re-imaging optics to refocus the telescope beam onto our slicer). The cut through of the liquid nitrogen vessel in Fig. 3 shows an inner support rib. The liquid nitrogen worksurface is suspended from the warm vacuum vessel by G-10 fiberglass stand-offs which provide high mechanical stiffness and low thermal conductivity. The liquid nitrogen container is designed for a cryogen holding time of about 28 hours.

The 35 liter main liquid helium reservoir provides cooling for the inner radiation shields and the liquid helium optical bench. The liquid helium optical bench, suspended from the liquid nitrogen worksurface by G-10 tabs, mechanically supports and cools all of the optical components after the calibration system (excluding the detectors). The expected cryogen holding time for the main liquid helium reservoir is up to 50 hours.

Since the detector arrays require operating temperatures below 4K,[6] they are mounted to a small 2.8 liter superfluid helium tank, which is suspended by carbon fiber tabs from the liquid helium optical bench. This tank is pumped in order to reach a temperature of $\sim$ 2K. The expected maximum holding time for the pumped liquid helium tank is about 18 hours. To ensure safe operation during flight, all cryogen vessels are provided with coaxial neck tubes and warm pressure relief valves.

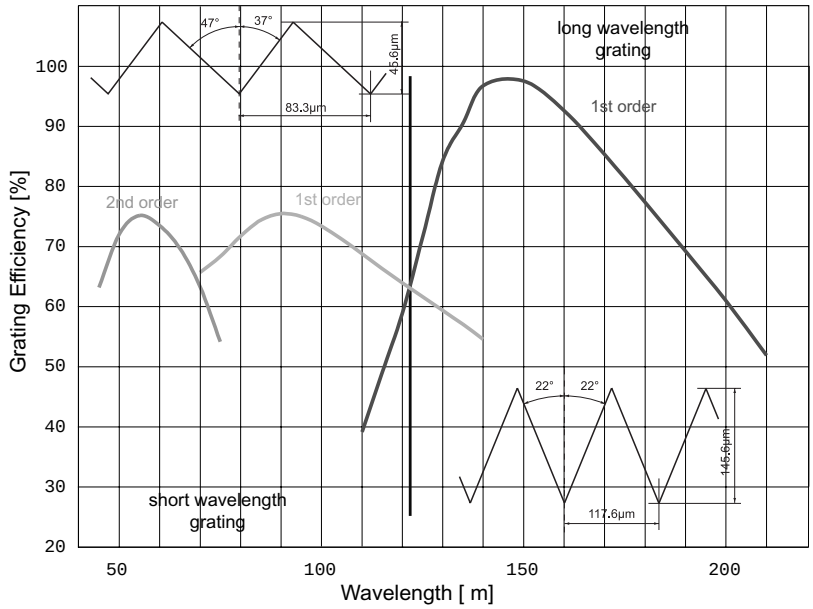

Figure 5. Efficiency of the gratings as a function of wavelength and diffraction order. The insets shown are the grating profiles: Blue channel on the left and Red channel on the right.

3.2. Optical Components

Although we discuss in detail the optics in this volume,[11] we will briefly review the overall optical layout in FIFI LS here. Fig. 4 shows a 3D model of the FIFI LS optical path. In this view, the light from the telescope enters from the left, coming into the plane of the image. The two channels share the K-Mirror, re-imaging optics, and the calibration optics that provide a dual-temperature chopped source, all of which are on the nitrogen working surface. The two otherwise independent spectrometers are separated shortly after the Lyot stop in the helium working surface via a multi-layer air-gap/metal interference dichroic. The Red channel is towards the bottom of the figure and the Blue channel is towards the top of the figure. After the entrance optics and dichroic, the two wavebands have separate slicer mirrors, spectrometers (including individual grating drive systems), detectors, and read out electronics. Thus, FIFI LS is designed such that any problem in one channel will not affect the operation of the other channel.

3.3. Gratings

The two wavelength channels obviously need two separate, optimized gratings for operation. The Red channel covers less than an octave of wavelength, and can utilize a grating operated in only 1st grating order, but the Blue channel must use 1st and 2nd order to fully cover its wavelength band. The observing wavelength is selected by physically moving the grating, or rather tilting it, which changes the angle of the incident beam. In order to maximize the efficiency of the two gratings, the reflective grating profiles were extensively modeled using a program that fully solves the Maxwell equations for periodic boundary conditions, PCGrate 1E version 3.0.[13] We require the gratings to have maximum efficiency at astronomical relevant wavelengths ($\sim$60 μm and $\sim$160 μm), yet the efficiency should be relatively flat across the entire band of interest (a redshifted galaxies needs to be observed at offset wavelengths), and finally, the groove profile should be relatively easy to manufacture using a diamond-tooled milling machine– generally triangular shaped. The final profile with the calculated efficiency is shown in Fig. 5 where the Red channel was optimized for only 1st order operation and the Blue channel for the even combination of 1st and 2nd order. We use diamond milled aluminum gratings from Hyperfine Inc.

3.3.1. Grating Position Read-out

For sub-arcsecond measurement of the angular position, or tilt, of the gratings, we directly attached an Inductosyn^{TM} position transducer. An Inductosyn is effectively a transformer with the primary and secondary windings placed

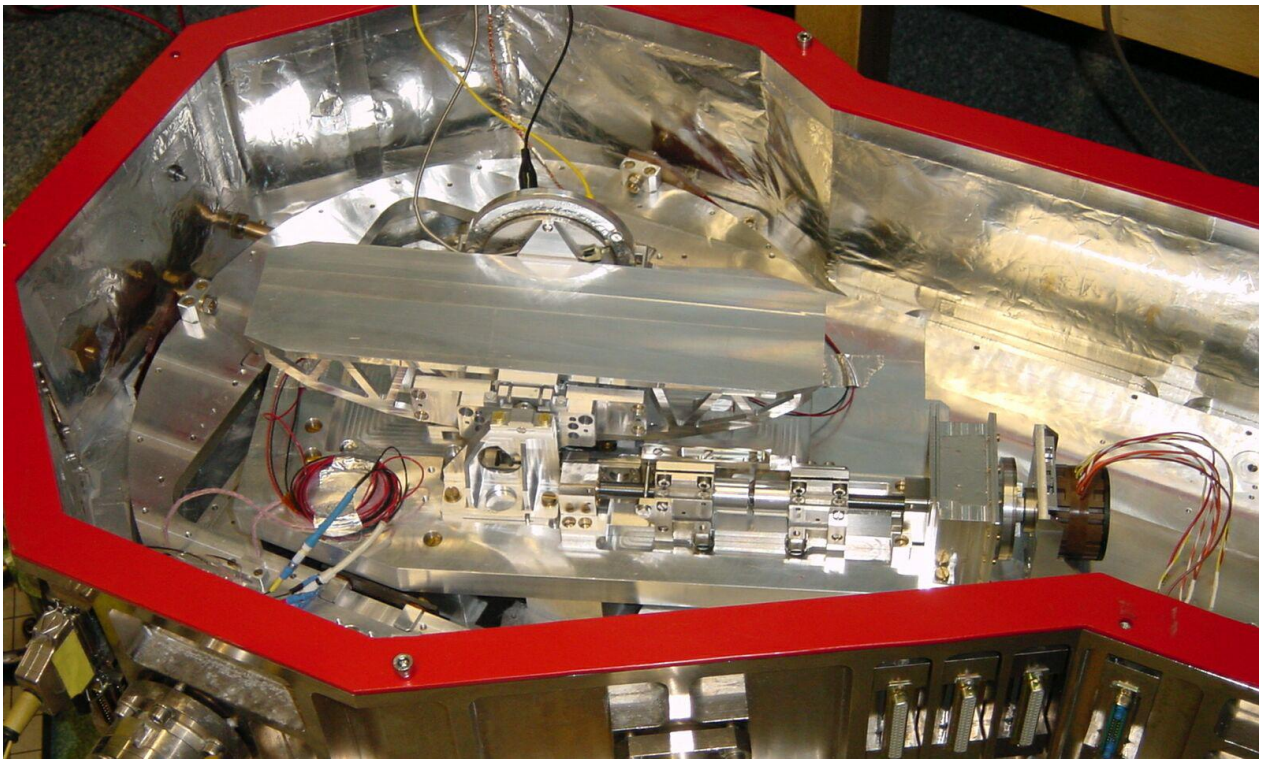

Figure 6. A grating blank in the mechanical grating drive test set-up. To the right is a stepper motor, kept at nitrogen temperatures. The roller screw mechanism is also clearly seen. The half rounded shape toward the top is the Inductosyn resolver. It is interesting to note that this one grating drive is being tested in the cryostat of our old KAO instrument FIFI, and the single grating does not even fit on the Helium worksurface.

on a rotor and stator, respectively. The winding pattern on the rotor is excited by a 10 kHz signal, while on the stator, there are two periodic patterns that are spatially 90° out of phase with each other. In operation, the rotor and stator windings inductively couple such that the two output signals from the stator have amplitudes which vary as the sine and cosine functions based on the relative position in each winding cycle. The relative amplitudes of the two transducer outputs are a measure of the actual position of the grating within one period, with proper initial calibration. Both signals are amplified separately in a low-noise amplifier stage and translated into 16 bit digital position data by a Resolver-to-Digital Converter. Since the transducer output produces a rollover of the position data every 1.4°, an additional loop counter keeps track on the position data over the full 40° tilting range of the grating.

3.3.2. Grating Mechanical Layout

To reach a spectral resolution of ∼100 - 250 km/s, the grating has to be moved and controlled at liquid helium temperatures with a precision of less than 3″ (corresponding to 1/10 a pixel) while maintaining an optical surface mechanical stability of 50 marcsec/$\sqrt{Hz}$. The grating is actuated by a two stage tilting mechanism. The first stage, for coarse positioning, consists of a support structure connected to the bottom of the grating. The support structure is driven by a roller-screw lever arm mechanism (a so-called sine-bar mechanism) that tilts the grating via a push-pull movement. The roller screw is driven by a stepper motor at liquid nitrogen temperature that is thermally isolated from the grating by a magnetic feed-through. For this low temperature operation (4 K), we used Dicronite^{TM} on all moving surfaces as a dry lubricant.

The second stage of the grating drive, for fine positioning, utilizes 2 PZT (Plumbum Zirconate Titanate) stacks in series to drive the grating with respect to the support structure through a directly attached lever arm. The PZT movement is controlled with a PC/104 board using a PID control software loop with a bandwidth of up to

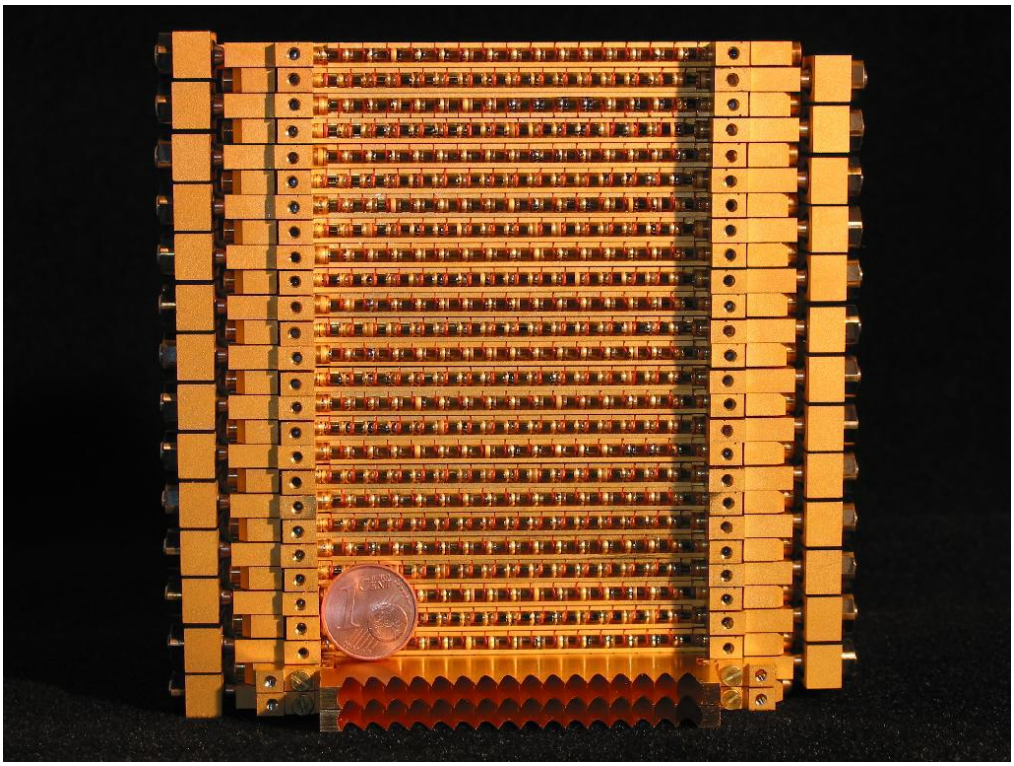

Figure 7. The final FIFI LS flight detector modules– 25 + 2 spares. All but two are shown without their lightcones so that the individual pixels and alignment pieces can be better seen. Included in the picture is a 1 Euro cent piece for scale. Together with our satellite project PACS,[8] this is the largest far-infrared photoconductor array ever made.

a few hundred Hz. Additionally, an eddy current damping system is mounted to the grating to minimize in-flight vibrations of the airplane, which are a perpetual source of error on airborne experiments, especially affecting moving parts where resonant modes can increase motion error to an unacceptable value. The entire system is now being tested in the cold inside the old FIFI cryostat, see Fig. 6. Preliminary results show that we can easily meet our specifications.

3.4. Detectors

Although the FIFI LS detectors, and photoconductor detectors in general, are discussed at this SPIE conference,[8] we will present a quick overview of the FIFI LS detectors. As mentioned above, FIFI LS uses two detector arrays to cover the 42 - 110 μm and 110 - 210 μm wavelength bands.[6] We chose to use Gallium-doped Germanium photoconductor detectors since they are proven to be very sensitive in the wavelength range 40 - 120 μm, and, with the application of $\sim$ 600 N mm^{-2} of stress, their wavelength sensitivity shifts to 100 - 220 μm.[6,12,14] Thus, FIFI LS uses two 25 $\times$ 16 Ge:Ga detector arrays, one stressed and one slightly stressed,[6] directly corresponding to the Red and Blue channels respectively.

As shown in Fig. 7, we already have constructed the Red detector, and it has passed our first cool-down tests. The Noise Equivalent Power (NEP) and quantum efficiency have not yet be tested on these flight models, but they have been investigated in some prototype modules[6] using conventional transimpedance amplifiers. We find a NEP of about 1.5 $\times$ 10^{-16} W Hz$^{-1/2}$ at 10^{-12} W per pixel background that is relatively flat at bias voltages of 30 to 60 mV. In the range of the flat NEP, the quantum efficiency, as derived from assuming background limited performance, of the entire system, including the detector integrating cavity and lightcones, ranges from 25% to 35%. This is significantly higher than the quantum efficiency of the detectors in our KAO instrument FIFI ($\sim$ 20%).[12] The Blue detectors are currently being designed using a very similar module concept as the Red detectors with a softer spring

Wavelength Range		42 - 110 μm	110 - 210 μm
Pixel size		$6''\times 6''$	$12''\times 12''$
Field of view 5×5 pixels		$30''\times 30''$	$60''\times 60''$
Resolution ($c\Delta\lambda/\lambda$)		40 -150 km/s	100 -240 km/s
Instantaneous Vel. coverage		1300 - 3000 km/s	1300 - 3000 km/s
Point source det. limit	$\lambda = 50\mu$m	3.9×10^{-17} W/m^2	.....
(5σ in 1 hr)	$\lambda = 100\mu$m	2.2×10^{-17} W/m^2	.....
	$\lambda = 150\mu$m	.....	1.4×10^{-17} W/m^2
	$\lambda = 200\mu$m	.....	1.8×10^{-17} W/m^2

Table 1. FIFI LS performance specifications.

mechanism. The new design is beginning to undergo initial testing showing that the pixel alignment mechanism is sufficient.

4. SCIENTIFIC CAPABILITIES

The combination of the dual integral field spectroscopy in two wavelength bands, the medium resolving power, and the diffraction limited imaging capabilities make FIFI LS well suited to address a number of astrophysical problems. Table 1 lists the expected sensitivity and spatial parameters of the instrument for observers. To summarize, FIFI LS employs two fixed pixel sizes of $6''$ (Blue Channel– short wavelength spectrometer) and $12''$ (Red Channel– long wavelength spectrometer), respectively, determined by the image slicer. The two 5 × 5 pixel fields of view have the same pointing center and are observed simultaneously with two Ge:Ga photoconductor arrays. Observing wavelengths are adjusted by tilting the Littrow mounted grating in each channel. Spectral coverage of $\sim$ 1500 km/s around a selected far-infrared line is obtained simultaneously for all 25 spatial pixels.

REFERENCES

1. A. Poglitsch, J.W. Beeman, N. Geis, R. Genzel, M.H.E.E. Haller, J. Jackson, M. Rumitz, G.J. Stacey, & C.H. Townes, *Int J. IR & Millimeter Waves*, 12 (1991)
2. N. Geis, R. Genzel, M. Haggerty, F. Herrmann, J. Jackson, S.C. Madden, T. Ncola, A. Poglitsch, M. Rumitz, G.J. Stacey, R. Timmermann, and C. H. Townes, ASP Conference Series 73, Airborne Astronomy Symposium on the Galactic Ecosystem, M.R. Haas, J.A. Davidson, & E.F. Erickson eds. (1995)
3. N. Geis, A. Poglitsch, W. Raab, D. Rosenthal, G. Kettenring, T. Henning, & J.W. Beeman, SPIE Proc. Infrared Astronomical Instrumentation, A.M. Fowler ed. (1998)
4. W. Raab, N. Geis, L. Looney, A. Poglitsch, D. Rosenthal, A. Urban, T. Henning, & J.W. Beeman, SPIE Proc. 3759 Infrared Spaceborne Remote Sensing VII, B. Andersen ed. (1999)
5. L.W. Looney, N. Geis, R. Genzel, W.K. Park, A. Poglitsch, W. Raab, D. Rosenthal, A. Urban, & T. Henning, SPIE Proc. 4014 Airborne Telescope Systems, R. Melugin & H.P. Röser eds. (2000)
6. D. Rosenthal, J.W. Beeman, N. Geis, L. Looney, A. Poglitsch, W.K. Park, W. Raab,, & A. Urban, Proc. SPIE Proc. 4014 Airborne Telescope Systems, R. Melugin & H.P. Röser eds. (2000)
7. R. Hönle et al. in prep.
8. A. Poglitsch, R.O. Katterloher, R. Hönle, J.W. Beeman, E.E. Haller, H. Richter, Haegel, N.M., & A. Krabbe, SPIE Proc. 4855 (2002)
9. W. Benesch & J. Strong, J. Opt. Soc. Am. 41 (1951)
10. A. Krabbe, L. Weitzel, H. Kroker, L. E. Tacconi-Garman, M. Cameron, N. Thatte, G. Samann, T. Boeker, R. Genzel, & S. Drapatz, Proc. SPIE 2475, Infrared Detectors and Instrumentation for Astronomy, A. M. Fowler ed. (1995)
11. W. Raab, L.W. Looney, A. Poglitsch, N. Geis, R. Hönle, D. Rosenthal, R. Genzel, Proc. SPIE 4857, this volume (2002)

12. G.J. Stacey, J.W. Beeman, E.E. Haller, N. Geis, A. Poglitsch, & M. Rumitz, Int. J. Inf. Mill. Wave, 13, 1689 (1992)
13. J. Goray SPIE Proc. 2532, 427 (1995)
14. J.W. Beeman & E.E. Haller, Inf. Phys. Tech., 35, 827 (1994)